

Ginga observations of Cygnus X-2

R.A.D. Wijnands¹, M. van der Klis¹ E. Kuulkers² K. Asai³ G. Hasinger⁴

¹ Astronomical Institute “Anton Pannekoek”, University of Amsterdam and Center for High Energy Astrophysica (CHEAF), Kruislaan 403, 1098 SJ Amsterdam, The Netherlands

² ESA/ESTEC, Astrophysics Division (SA), P.O. Box 229, 2200 AG Noordwijk, The Netherlands

³ Institute of Space and Astronautical Science, 1-1 Yoshinodai 3-chome, Sagamihara, Kanagawa 229, Japan

⁴ Astrophysikalisches Institut Potsdam, An der Sternwarte 16, 14482 Potsdam, Germany

Received ; accepted

Abstract. We have analysed all available X-ray data on the low-mass X-ray binary Cygnus X-2 obtained with the Ginga satellite. A detailed analysis of the spectral and fast timing behaviour of these 4 years of data provides new insights in the behaviour of this Z source. We confirm the previously observed recurrent patterns of behaviour in the X-ray colour-colour and hardness-intensity diagrams consisting of shifts and shape changes in the Z track. However, we find a continuous range of patterns rather than a discrete set. The source behaviour in the diagrams is correlated with overall intensity, which varied by a factor of 1.34 in the Ginga data. We find that when the overall intensity increases, the mean velocity and acceleration of the motion along the normal branch of the Z track increase, as well as the width of the normal branch in the hardness-intensity diagram. Contrary to previous results we find that, during different observations, when the source is at the same position in the normal branch of the Z track the rapid X-ray variability differs significantly. During the Kuulkers et al. (1996a) “medium” level, a normal branch quasi-periodic oscillation is detected, which is not seen during the “high” overall intensity level. Also, during the high overall intensity level episodes the very-low frequency noise on the lower normal branch is very strong and steep, whereas during the medium overall intensity level episodes this noise component at the same position in the Z track is weak and less steep. The explanation of the different overall intensity levels with a precessing accretion disk is difficult to reconcile with our data. Furthermore, we found that the frequency of the horizontal branch quasi-periodic oscillation decreases when Cygnus X-2 enters the upper normal branch, giving a model dependent upper limit on the magnetic field strength at the magnetic equator of $\sim 8.5 \times 10^9$ G. We also report five bursts, with durations between two and eight seconds, whose occurrence seems to be uncorrelated with location in the Z track, overall inten-

sity level or orbital phase. The burst properties indicate that they are not regular type I bursts.

Key words: accretion, accretion disks – stars: individual: Cyg X-2 – stars: neutron – X-rays: stars

1. Introduction

Cygnus X-2 (discovered by Bowyer et al. 1965) is a very well studied bright low-mass X-ray binary (LMXB). Hasinger & van der Klis (1989) classified the brightest LMXBs into two sub-classes, i.e. the “Z” sources and the “atoll” sources, on the basis of their correlated X-ray spectral and fast timing behaviour. Cygnus X-2 was classified as a Z source. In the X-ray colour-colour diagram (CD) Z sources trace out a Z shaped track and move smoothly, without jumps, through the branches. In all the six known Z sources, except GX 349+2, three branches have been identified, the horizontal branch (HB), the normal branch (NB) and the flaring branch (FB). The transition between the HB and the NB is called the hard vertex, and between the NB and the FB the soft vertex. The variation of one single parameter, i.e. the mass transfer rate to the compact object (\dot{M}), is thought to produce the tracks (e.g. Hasinger & van der Klis 1989, Lamb 1991).

Recent studies of EXOSAT data of the Z sources (see Kuulkers et al. 1994a, 1996a,b; Kuulkers & van der Klis 1996) indicate that the Z sources can be divided into two groups, the Cyg-like sources (Cyg X-2, GX 5-1 and GX 340+0) and the Sco-like sources (Sco X-1, GX 349+2 and GX 17+2). The Cyg-like sources show motion of the Z pattern in the colour-colour diagram and the hardness-intensity diagram (HID), their HBs are horizontal, and when the sources are on their short FBs the X-ray intensity generally decreases. The Sco-like sources, instead, do not display significant motion of their Z pattern in the

Send offprint requests to: R.A.D. Wijnands, e-mail: rudy@astro.uva.nl

CD, their HBs are almost vertical, and the X-ray intensity increases when they move onto their extended FBs. It was proposed (see Kuulkers & van der Klis 1995b, and references therein) that the Sco-like sources are viewed face-on (low orbital inclination) and the Cyg-like sources more edge-on (higher orbital inclination), and that the motion of the Cyg-like sources could be caused by accreting material, such as a precessing accretion disk getting into the line of sight.

Theoretical studies (Psaltis et al. 1995) indicate that a difference of magnetic field strength can explain some of the differences between the Cyg- and the Sco-like sources. In their model, the Cyg-like sources have a somewhat higher magnetic field strength ($B \sim 5 \times 10^9$ Gauss) than the Sco-like sources ($B \sim 10^9$ Gauss). Their so-called unified model can explain the Z tracks in the CDs and HIDs and the difference in the Z shapes between the Cyg-like and Sco-like sources. However, no explanation is given for the fact that the Cyg-like sources display motion of the tracks, whereas the Sco-like sources do not.

Cygnus X-2 shows the most pronounced motion of the Z pattern in the CD and the HID of all Z sources. One of the first observations of Z pattern motion in the HID was found by Vrtillek et al. (1986) using Einstein MPC data. They observed a factor of two increase in intensity between different epochs but also an increase of the intensity on time scales less than a day. At that time the Z track behaviour of Cygnus X-2 was not yet known, so they interpreted the variations as due to orbital effects. Nowadays we know that most of the intensity variations of Cygnus X-2 are due to the non-periodic motion of the source through the Z track, and most likely associated with changes in M . However, not all intensity variations that were found by Vrtillek et al. (1986) can be explained in this manner. In their Fig. 2, three branches are present which now can probably be identified as NBs. These branches are shifted with respect to each other, making this in retrospect the first indication that Cygnus X-2 displays motion of the Z-track in the HID.

Clear evidence for Z track motion in the CD and the HIDs was found when different EXOSAT observations of Cygnus X-2 were compared with each other (Hasinger et al. 1985b, Hasinger 1987, 1988). Hasinger (1987) discussed six EXOSAT observations of Cygnus X-2. He found that the Z tracks of different observations were displaced in the HIDs with respect to each other. Hasinger et al. (1985b) and Hasinger (1988) reported a state of Cygnus X-2 with very low count rates. The count rates, especially in the high energy bands, flared and the spectrum was hard. In the CD this observation looked like a large FB, and it is displaced to harder colours with respect to other Cygnus X-2 EXOSAT observations (see also Kuulkers et al.

Vrtillek et al. (1988) investigated the long-term temporal variability of Cygnus X-2 using six different instruments on three satellites (OSO 8, HEAO 1, and Einstein).

Three count rate states between 2 and 10 keV were found. During the lowest state the spectrum was harder than during the other two states.

The motion of the Z trough the CD and HID was again reported in early Ginga observations of Cygnus X-2 reported by Hasinger et al. (1990). They found that the Z track in the HID during the October 1988 observation was shifted to higher intensities (by a factor two) with respect to the July 1988 observation. In the CD the Z track of the October 1988 observation was shifted downward parallel to the NB with respect to the July 1988 observation. The shape of the Z track in both the CD and the HID was different between these two observations. During the July 1988 observation the Z track performed a loop in the HID at the NB-FB transition, such that along the FB the source first rose in intensity and later decreased. During the October 1988 observation no such loop was found. Instead, along the FB the source immediately started to decrease in intensity. In the CD of the July 1988 observations the HB is diagonal and the FB is large. In the October 1988 CD the HB is horizontal and the FB is very small.

Kuulkers et al. (1996a) reanalysed all EXOSAT observations of Cygnus X-2. They also reported motion of the Z pattern and different shapes of the Z track. They compared their results with all previous reports on Cygnus X-2, and described the phenomenology in terms of three different intensity levels (possibly part of a continuous sequence). In the rare low level Cygnus X-2 displays a hard spectrum at the lowest intensities. These episodes seemed to occur at binary phases 0.8-0.2 (with phase 0.0 defined as the X-ray source superior conjunction), however not in each orbital cycle. Vrtillek et al. (1988) and Kuulkers et al. (1996a) discussed various possible explanations, e.g. that at these times the secondary hides its heated face and/or part of our view of the inner disk region, so that most of the observed radiation then comes from a scattering hot corona surrounding the inner accretion disk, or that a tilted disk or a hot spot at the outer disk hide much of the inner disk region from our view. The other two intensity levels were called the medium and the high level. A periodicity in the occurrence of these intensity levels could not be found. The shape of the Z track in the HIDs was dependent on these intensity levels. As the source moves onto the FB during high level episodes, the intensity immediately starts to decrease and the FB in the HID is almost horizontal. They called this a 'colour-independent' dip. When the source moves up the FB during medium level episodes the intensity first increases and then decreases. The FB in the HID is also pointed upwards and therefore referred to as a 'colour-dependent' dip. No Z track was observed during the low level.

The fast timing behaviour of Z sources is closely related to the position of the sources in the CD and HID (Hasinger & van der Klis 1989). On all branches a very-low frequency noise (VLFN) and a high frequency noise (HFN)

Table 1. Log of the observations

Nr	start (UT)	end (UT)	total time (h)	mode	binary phase ^a
1	1987-06-07 15:29	1987-06-10 21:43	6.74	MPC1, MPC3, PC	0.70-0.03
2	1988-06-10 05:33	1988-06-14 04:05	28.80	MPC2, MPC3, PC	0.14-0.54
3	1988-10-06 00:50	1988-10-07 23:40	18.24	MPC1, MPC2, MPC3, PC	0.12-0.30
4	1989-10-22 01:41	1989-10-24 01:06	8.07	MPC1, PC	0.81-0.01
5	1990-11-30 16:13	1990-12-02 13:31	2.32	MPC1, MPC3	0.91-0.11
6	1991-05-15 01:16	1991-05-16 10:00	7.83	MPC1, MPC3	0.71-0.85
7	1991-06-09 18:26	1991-06-11 06:41	11.32	MPC1, MPC2, MPC3	0.33-0.48

^a orbital phase using the ephemeris given by Crampton & Cowley (1980), see Kuulkers et al. (1996a) note 4.

component in the power spectra can be identified. On the horizontal and normal branches also low frequency noise (LFN) can be identified which decreases in amplitude from the HB to the upper normal branch and disappears on the lower normal branch. Quasi-periodic oscillations (QPOs) are found on the horizontal branch (called HBOs) with a frequency from ~ 12 Hz at the left end of the HB up to ~ 55 Hz near the hard vertex, and then remains constant upto halfway the normal branch. However, Wijnands et al. (1996a) found a decrease of the frequency of what is probably the HBO down the NB in GX 17+2. On the NB QPOs (NBOs) are observed with a frequency between 5–7 Hz. Sometimes the HBO is seen simultaneously with the NBO, indicating different mechanisms are responsible for these QPOs. On the flaring branch sometimes a QPO (FBO) is seen with a frequency near 7 Hz at the beginning of the FB, but rapidly increasing in frequency up to ~ 20 Hz further up the FB. The 7-20 Hz flaring branch QPO has not been found on Cygnus X-2. However, Kuulkers & van der Klis (1995a) detected a QPO on the FB of Cygnus X-2 with a frequency of 26 Hz. This QPO was found in an intensity dip on the FB and is believed to be a different phenomenon from the 7-20 Hz FBO.

Two Z sources are known to show bursts. GX 17+2 (Tawara et al. 1984; Kahn & Grindlay 1984; Sztajno et al. 1986; Kuulkers et al. 1994b, 1996b) shows bona fide type I burst (thermonuclear flashes on the neutron star surface, Hoffman et al. 1978). In Cygnus X-2 burst-like events have been reported (Kahn & Grindlay 1984; Kuulkers et al. 1995). Kuulkers et al. (1995) detected 9 burst-like events in the archival EXOSAT data of Cygnus X-2. These burst-like events had a short duration ($t_{\text{burst}} \sim 3$ s), did not show evidence for cooling, and did not occur in specific regions of the Z track. To date it is unclear whether these burst-like events are genuine type I bursts.

In this paper we present an uniform analysis of all available data obtained by the Large Area Counter (LAC) instrument on board the Ginga satellite.

2. Observations and Analysis

2.1. The satellite and the observations

Cygnus X-2 was observed with the Ginga satellite (Makino and the ASTRO-C team 1987) during 7 observations. For a log of the observations we refer to Table 1. Due to Earth occultations and the high background in the South Atlantic Anomaly (SAA) the observations were broken up into many pieces with a length of several tens of minutes.

The LAC instrument (Turner et al. 1989) on board Ginga was used in several different observation modes : the MPC1, MPC2, MPC3 and the PC mode. In the MPC1 and the MPC2 (hereafter MPC1/2) modes the source was observed in 48 photon energy channels and the time resolution ranged from 62.5 ms to 16 s. In the MPC3 mode the source was observed in 12 channels with a best high time resolution of 7.8 ms. In the PC mode only four overlapping channels were used and the time resolution was 1 or 2 ms. By manipulating the coarse gain (CG) amplifier, which had two levels, the energy range could be set to either 0.5–37 keV (low CG level) or to 0.3–18.7 keV (high CG level). By changing the high voltage (HV) levels the energy range could be extended to even higher energies (e.g. up to 60 keV). Due to these different CG amplifier settings, HV level settings and lower discriminator settings (see Turner et al. 1989) different sets of energy channels were used at different times.

Generally the satellite attitude control system kept the viewing direction within 30 arcmin from the position of Cygnus X-2, which corresponds to a collimator transmission of $\gtrsim 70\%$. The systematic error in the observed count rates due to uncertainties in the collimator transmission is of the order of a few percent (Hertz et al. 1992). Due to, e.g., a long period without attitude control measurements the offset angle sometimes increased causing the collimator transmission to decrease to about 40%. The LAC collimator shows energy-dependent transmission effects due to reflection of soft X-rays (below ~ 6 keV) from the collimator walls at large offset angles (Turner et al. 1989). This low energy reflection was not taken into account when the intensities were corrected for collimator transmission (Sect. 2.2), which gives rise to an overestimation of the

Table 2. The energy bands used to create colour-colour and hardness-intensity diagrams. We used the following definitions of the colours : Soft Colour = $^{10}\log(\text{Band 2} / \text{Band 1})$, Hard Colour = $^{10}\log(\text{Band 3} / \text{Band 2})$. The intensity is the count rate in the energy range given in column 6

Observation period	Mode	Band 1 keV	Band 2 keV	Band 3 keV	Energy range used for the total intensity keV
1987 and 1988	MPC1/2 and MPC3	2.3–4.7	4.7–7.0	7.0–18.6	2.3–18.6
1991	MPC1/2	2.3–4.7	4.7–7.0	7.0–18.6	2.3–18.6
1991	MPC3	2.4–4.7	4.7–7.1	7.1–18.8	2.4–18.8
1989 and 1990	MPC1/2	2.9–4.8	4.8–6.7	6.7–19.0	2.9–19.0
1989 and 1990 ^a	MPC1/2 and MPC3	1.2–3.8	3.8–7.6	7.6–19.0	1.2–19.0
1987	PC	0.6–2.9	2.9–9.1	7.9–12.3	0.6–9.1 + 0.8–12.3
1988	PC	0.8–2.9	2.9–9.1	7.9–12.3	0.8–9.1 + 0.8–12.3
1989	PC	1.2–5.7	1.2–15.7	5.7–17.9	1.2–17.9 + 1.2–15.7

^a These bands were used in order to determine in which part of the Z Cyg X-2 was during the 1990 MPC3 observation (see text).

count rates for the lowest energy channels. When we encountered data with a collimator transmission below $\sim 60\%$ we used Figs. 13 and 14 of Turner et al. (1989) in order to correct the count rates below 6 keV. Usually this means that the count rates were corrected for an overestimation of 3–4%. Sometimes the offset angle was even higher and the collimator transmission came below $\sim 20\%$. At such high offset angle the collimator response is independent of incident photon energy (Turner et al. 1989). However, at these times the fractional uncertainty in the collimator transmission, and thus in the corrected count rates, due to aspect jitter is $\gtrsim 15\%$ (Hertz et al. 1992). For this reason, we did not use any data with a collimator transmission $\lesssim 40\%$ in our analysis.

2.2. Colour-colour and hardness-intensity diagram analysis

For our studies of the CDs and the HIDs we used data rebinned to a time resolution of 4 seconds, which were background subtracted and corrected for deadtime and aspect using the ISAS analysis system. The PC binned data were not corrected for background because no good background determinations are available for them. The 16 s resolution MPC1 data of the November 1990 and June 1991 observations had multiple register overflows and were left outside our analysis. The 4 s resolution MPC1 data of the June 1987, the October 1989, the May/June 1991 observations and the 2 s resolution MPC2 data of the June/October 1988 and the June 1991 observations had single overflows and the true count rates could be recovered.

In order to make CDs and HIDs we calculated the soft colour, the hard colour and the total intensity. The definitions of those quantities and the energy bands used in order to calculate them, are given in Table 2. Instead of the colours and intensities, usually used in the literature, we used the logarithmic value of those quantities. Any pro-

cess which influences the intensity in the specified energy bands by multiplication, i.e. the instrumental response, produces only a shift in the CD and the HIDs. Using logarithmic values of the colours and the intensity therefore makes it easier to compare data of the same source obtained by different instruments, by simply shifting the diagrams. Also, the S_z parametrization (Sect. 2.3) in this way does not depend on the actual values of the quantities or the count rates, but only on their changes. It can now be used not only for the CD but for the HIDs as well.

Usually the total intensity was taken as the sum of the count rates in the same energy bands as were used to calculate the colours. However, for the PC data of the 1987 and the 1988 observations the total intensity was defined as the count rate in all four energy channels. For the 1989 PC data the count rates in the three lowest energy channels were summed, as the fourth channel only contained background photons. The lowest energy boundary of the 1987 PC data differs slightly from the lowest boundary in the 1988 PC data (Table 2). The effect on the Z in the CD and HID is negligible and therefore we discuss the 1987 and 1988 PC data together. The 1989 PC data is discussed separately because of the different energy boundaries (see below).

In order to compare the MPC1/2 data with the MPC3 data we rebinned the MPC1/2 data to 12 channels using the same energy boundaries as the MPC3 data. Although in the 1991 observations the MPC3 data had slightly different energy boundaries compared to the MPC1/2 data (Table 2), the difference was small and had no significant effect on the place of the Z in the CD and HID.

Due to the HV and CG levels of 1989 and 1990 observations (energy range 1–60 keV) the energy boundaries of their spectral channels differ from those of the other five observations. Due to the broad energy channels the energy boundaries of these observations could not be successfully interpolated to the boundaries of the others. Therefore, we

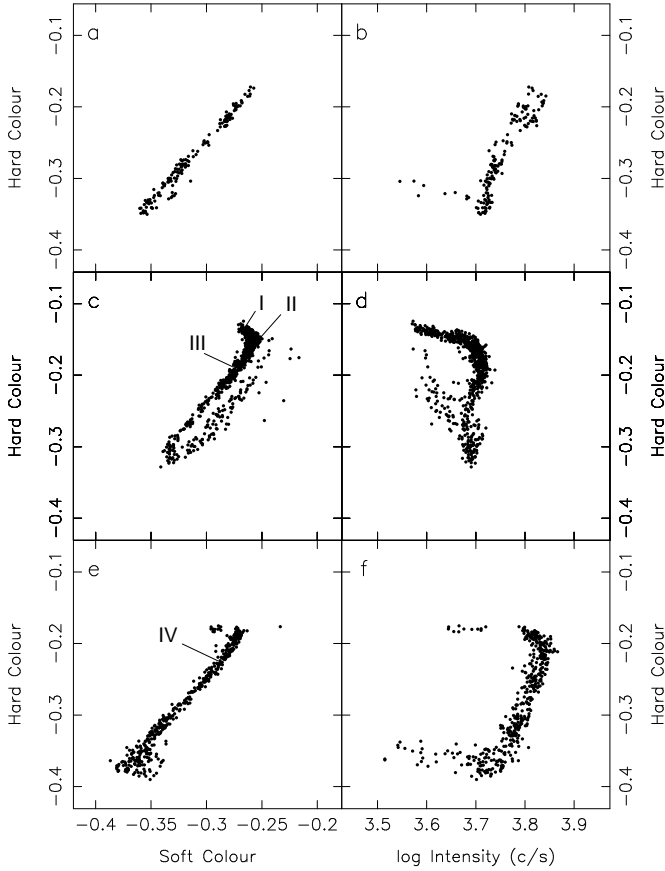


Fig. 1. The June 1987, June 1988, and October 1988 observations. MPC modes: **a**, **c**, and **e** are the colour-colour diagrams and **b**, **d**, and **f** are the hardness-intensity diagrams for the June 1987, June 1988 and October 1988 observation, respectively. For the definitions of the colours and the intensity see text and Table 2. The position of the I, II and the III (c) indicate the position in the Z track where the three June 1988 burst occurred. The position of the IV (e) indicates where the October 1988 burst occurred

discuss the 1989 and 1990 observations separately from the other observations. In order to get an approximately uniform analysis we took for the MPC1 mode data colours which resembles the colours used in the other observations.

2.3. S_z parametrization

Hasinger et al. (1990) introduced the concept of rank number of the Z track in the CD. This concept was refined by Hertz et al. (1992) and by Dieters & van der Klis (1996). Here we use the method described by Dieters & van der Klis (1996) for the measurement of the position along the Z, with the difference that we perform all operations on the logarithmic colours and intensity values (see Sect. 2.2). We therefore transform the two logarithmic colour coordinates (hard colour and soft colour) into the coordinates

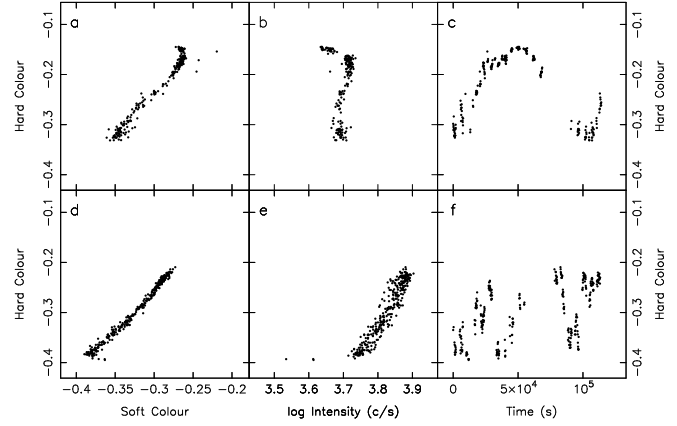


Fig. 2. The May 1991 and June 1991 observations. MPC modes: **a** and **d** are the colour-colour diagrams, **b** and **e** are the hardness-intensity diagrams, and **c** and **f** are the hard colour curves for the May and June observations, respectively

S_z (the distance along the Z track) and D_z (the distance perpendicular to the Z track). We also calculated the velocity (V_z) and the acceleration (A_z) along the Z track, as defined as

$$V_z(i) = [S_z(i+1) - S_z(i-1)]/[T(i+1) - T(i-1)], \quad (1)$$

where $S_z(i)$ is the position in the Z track on time $T(i)$, and

$$A_z(i) = [V_z(i+1) - V_z(i-1)]/[T(i+1) - T(i-1)], \quad (2)$$

respectively (see also Dieters & van der Klis (1996)). The length of the NB is scaled to 1 and positions on the HB and FB are normalised to the length of the NB. The hard vertex corresponds to $S_z=1$, and the soft vertex to $S_z=2$. We applied the S_z parametrization also on the Z tracks in the HID. We obtained a different set of S_z and D_z values which we call S_z^{hid} and D_z^{hid} .

The distribution of D_z or D_z^{hid} is a measure for the thickness of the branches in the CD or HID, respectively. To quantify the thickness of the branches we calculated the sample standard deviation of the D_z and D_z^{hid} distributions using the method described in the Appendix. As a measure of the overall velocity and acceleration in the CD the standard deviations of the V_z and A_z distribution were used, again using the method outlined in the Appendix.

2.4. Power-spectral analysis

For the power-spectral analysis we used the MPC3 and PC data. We made FFTs of 128s data segments which resulted a frequency range of 0.0078–64 Hz (MPC3 7.8 ms resolution data) or 0.0078–256 Hz (PC 1.95 ms resolution data) in the power spectra. We calculated the FFTs for the energy interval 1.2–18.6 keV (June 1987, June/October 1988

and May/June 1991 MPC3 observations) or 1.2–19.0 keV (November 1990 MPC3 observation). For the PC mode we used the sum of the energy intervals 0.8–12.3 keV and 0.6–9.1 keV (June 1987), or 0.8–12.3 keV and 0.8–9.1 keV (June and October 1988), or 1.2–17.9 keV and 1.2–15.7 keV (October 1989).

The average level of the photon counting noise, modified by deadtime processes (the Poisson level), was estimated and subtracted using a counter deadtime of 206 μ s (MPC3 data) and 16.5 μ s (PC data) (see Mitsuda & Dotani 1989). In the resulting power spectra several components can be identified :

- very low frequency noise (VLFN), which we fitted with $A_V \nu^{-\alpha_V}$, where ν is the frequency, α_V is the power-law index and A_V the normalization constant.
- low frequency noise (LFN) and a high frequency noise (HFN), are fitted with $A_{L,H} \nu^{-\alpha_{L,H}} e^{-\nu/\nu_{L,H}}$, where $\alpha_{L,H}$ is the power-law index, $\nu_{L,H}$ the cut-off frequency, and $A_{L,H}$ the normalization constant, for the LFN (L) and HFN (H), respectively.
- HBO, its harmonic, NBO and FBO, are fitted with Lorentzians : $A_Q \frac{1}{(\nu - \nu_C)^2 + (\Delta\nu/2)^2}$, where ν_C the centroid frequency, $\Delta\nu$ the full width at half maximum (FWHM) of the QPO and A_Q the normalization constant.

The fractional rms amplitudes of the various noise components were determined by integrating their contribution over the following frequency ranges ; VLFN: 0.001–1 Hz, LFN: 0.01–100 Hz, HFN: 0.01–100 Hz. We note that variations in the collimator transmission could influence the VLFN (see e.g. the EXOSAT data of GX 17+2 [Kuulkers et al. 1996b]). The errors in the parameter values were calculated using an error scan through χ^2 space using $\Delta\chi^2 = 1$. Due to the poor statistics it was not always possible to fit a HFN component. When HFN was fitted we used $\alpha_H = 0$ because in Z sources this index was found to be consistent with zero (Hasinger & van der Klis 1989, Dieters & van der Klis 1996). The best way to examine the correlations between the timing behaviour and the position on the Z track is to select a small part of the Z track, using the S_z parametrization and determine what the corresponding timing properties are for that segment. However, our data did not allow this procedure as we did not have enough data at high time resolution for this procedure to give sufficient statistics. Therefore we first selected parts of the data that covered a relatively small S_z range and afterwards determined an average S_z value and range for the each data set.

3. Results : the spectral variations

The CDs and HIDs for all observations are presented in Figs. 1–6. Each point represents a time interval of 120 seconds of which $> 50\%$ contained data.

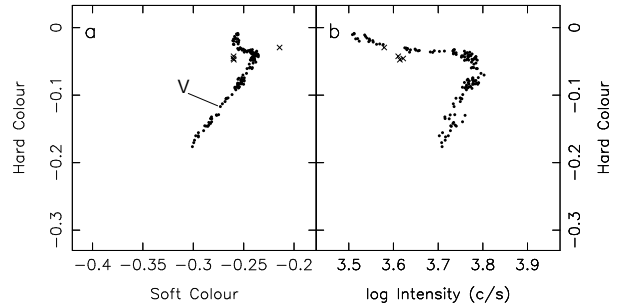


Fig. 3. The October 1989 and November 1990 observations. MPC1 modes: **a** is the colour-colour diagram and **b** is the hardness-intensity diagram. The dots (\bullet) are the October 1989 data, the crosses (\times) are the November 1990 data. The position of the V indicates where in the Z the October 1989 burst occurred

3.1. The 1987, 1988 and 1991 observations

3.1.1. June 1987

In both the CD and HID of the MPC-data (Figs. 1a and b) a NB can be seen. No HB is present. The FB is only just seen in the CD, but it is clearly visible in the HID. The count rate decreases as soon as the source enters this FB. In the HID, the upper NB is approximately twice as broad as the middle and lower NB. This broadening of the upper NB is not seen in the CD. The PC data (Figs. 5a and b) only show a NB. The June 1987 data were previously discussed by Mitsuda & Dotani (1989), however, they used 16-second data points. Due to the scatter induced by Poisson statistics they could not detect the broadening of the upper NB in the HID.

3.1.2. June 1988

This observation was already discussed by Hasinger et al. (1990). Parts of the data (from 1988 June 12 02:16 to 1988 June 13 08:49 UT and from 1988 June 14 01:29 to 03:59 UT) were obtained when the offset angle was about 1° , giving a collimator transmission of 40-60%. We corrected these data for the overestimation of the count rates in the low photon energy bands (Sect. 2.1). In the CDs of the MPC and PC data (Figs. 1c and 5c, respectively) clearly a HB, a NB and an extended FB are visible. The horizontal branch is not horizontal but diagonal. The HIDs of the MPC and PC data (Figs. 1d and 5d, respectively) also show all three branches. When the source moves into the FB, the count rate first slightly increases and then decreases.

3.1.3. October 1988

The CD and HID of the MPC data (Figs. 1e and f) were reported before by Hasinger et al. (1990). In the CD and HID all three branches are visible. The HB is really horizontal and when the source enters the FB the count rate

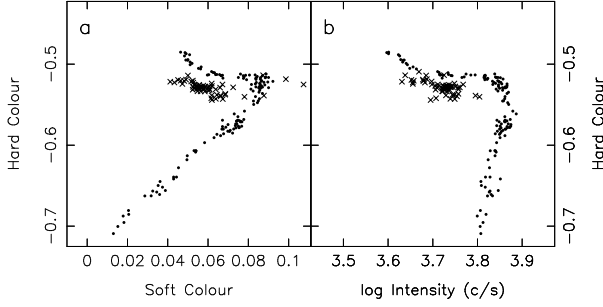


Fig. 4. The October 1989 and November 1990 observation. MPC1 and MPC3 modes: **a** is the colour-colour diagram and **b** is the hardness-intensity diagram. The dots (•) are the October 1989 data, the crosses (x) are the November 1990 data. The definitions of colours differ from the ones used in Fig. 3, see text and Table 2

decreases immediately. In the CD and HID of the PC data (Figs. 5e and f, not previously reported) three separate areas of points are visible. Comparing these figures with the MPC data of this observation, the upper and the middle area (indicated by HV and SV, respectively) are probably near the hard and soft vertices, respectively. This is confirmed by the fast timing analysis (see Sect. 4). The status of the third, lowest area (indicated by E) is unclear. The fast timing properties (see Sect. 4 and Table 5) suggest that Cygnus X-2 was near the soft vertex, either on the NB, or on the FB.

3.1.4. May 1991

Part of the data of this observation (from 1991 May 15 01:16 to 04:53 UT) was obtained when the offset angle was large and the collimator transmission low (40–60%). We attempted a correction to the low photon energy channels for the count rate overestimation (Sect. 2.1). During the time of low transmission, Cygnus X-2 seemed to be on the NB, as judged from the CD, but in the HID the same data points were displaced from the NB. Correcting the count rates for the low-energy flux overestimation was not enough to place the points exactly on the NB in the HID. In order to show more clearly the soft vertex and the beginning of the FB (see below) we did not include these points in the HID, and did not use them in our further analysis. In the CD (Fig. 2a) the HB is short and diagonal. No clear FB can be seen, but a full NB can. In the HID (Fig. 2b) the beginning of a FB can be seen, which is not made up of the points with the low collimator transmission. The count rate increases when the source enters the FB.

3.1.5. June 1991

During part of this observation (from 1991 June 10 10:06 to 16:02 UT) Cygnus X-2 was observed with a very large

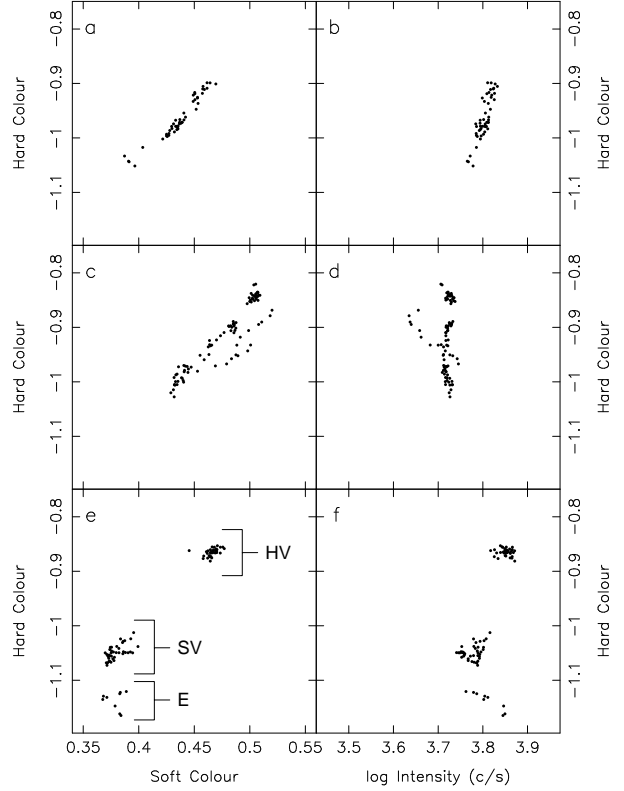


Fig. 5. The June 1987, June 1988 and October 1988 observations. PC mode: **a**, **c**, and **e** are the colour-colour diagrams and **b**, **d**, and **f** are the hardness-intensity diagrams for the June 1987, June 1988 and October 1988 observation, respectively. Most likely the parts of the Z in the CD of the October 1988 observation (**e**) indicated by HV and SV belong to the hard vertex and soft vertex, respectively. The state of the area indicated by E is unclear. See further text

offset angle and a collimator transmission of 10–20%. We did not include these data in our analysis because of the large uncertainties in the count rates (Sect. 2.1). The remaining data (Figs. 2d and e) show a clear NB, and a hint for a FB, which is most clearly seen in the HID. When examining the data at higher time resolution we see a more developed FB. No HB is observed. When the source moves onto the FB the count rate decreases immediately. The FB is approximately horizontal. Notice that the very broad NB in the HID corresponds to a narrow NB in the CD.

3.1.6. Comparison of the 1987, 1988 and 1991 observations

Comparing the five observations we find the following. The overall intensity level, defined as the mean count rate on the NB, changed by a factor of 1.34 between the observations. The lowest intensities were observed in June 1988 and May 1991, the highest intensities in October 1988 and June 1991. Intermediate intensities were observed in June 1987. Following the classification of Kuulkers et al.

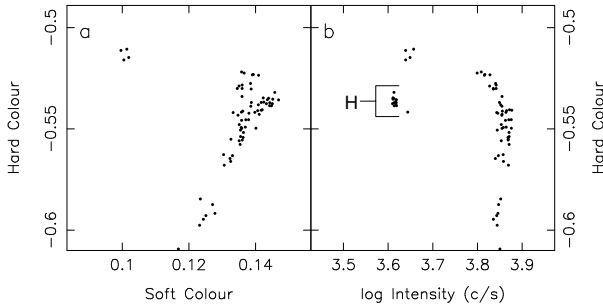


Fig. 6. *October 1989 observation.* PC mode: **a** is the colour-colour diagram and **b** is the hardness-intensity diagram. An harmonic of the HBO was seen in the part of the Z in the HID (**b**) which is indicated by the H. See also text

(1996a) our lowest overall intensities correspond to their “medium level” and our highest overall intensities to their “high level”. We shall adopt this terminology in what follows. As we also observe a level intermediate between these two, it is obvious from our data that the medium and high levels are probably part of a continuous range instead of a discrete set. We did not observe Cygnus X-2 when it was in the so-called “low level” (Kuulkers et al. 1996a). We confirm the previously reported (Hasinger et al. 1990; Kuulkers et al. 1996a and references therein) correlation between the shape of the Z in the CDs and HIDs and the overall intensity level.

In the *medium level* the HB is not horizontal but oriented under an $\sim 45^\circ$ angle in the CD. It is less steep in the HID. In the CD the HB is quite short compared to the NB. In the HID the HB and NB are of the same length. The NB is nearly exactly vertical in the HID, with almost no changes in intensity. The FB is very well developed in the CD, with large colour changes. In the HID, when the source enters the FB the count rate first increases, then, further up the FB, decreases. In the *high level* the HBs in both CD and HID are nearly horizontal. In the CD the HB is again short compared to the NB, while in the HID it is approximately the same length as the NB. The NB in the HID shows a positive correlation between hard colour and intensity. The FB in the CD is hardly visible, with hardly any colour changes. In the HID the FB is well developed and horizontal (little colour changes), and when the source moves onto the FB the count rate immediately decreases. The “*intermediate*” level shows characteristics of both the medium and the high level. Due to lack of data nothing can be said about the orientation of the HB during the intermediate level. The hard colour of the NB in the HID shows a positive correlation with intensity, similar to the high level, although not as clear. The FB in the CD is hardly visible, with small colour changes, also similar to the high level. When the source moves on the FB in the HID, which is not horizontal, this is similar to the medium level, the count rate immediately decreases

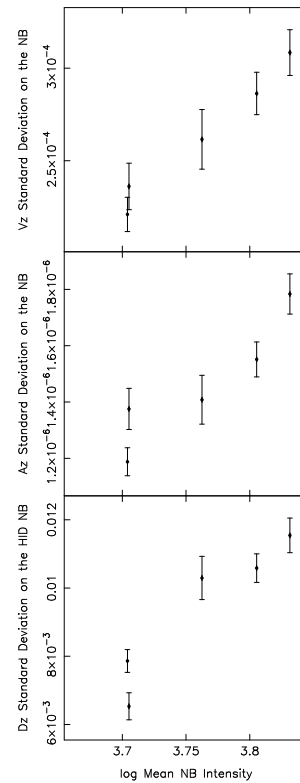


Fig. 7. Standard deviation of V_z (*upper*), A_z (*middle*) and D_z^{hid} (*lower*) on the NB against the log mean intensity (c/s) on the NB during the different observations

(like in the high level). In the CD and HID, the Z-track shifts downward (to softer colours), parallel to the NB in the CD, when the overall intensity level increases. In the medium level it is at its highest position (hard colour), in the intermediate level it is lower, and in the high level it is lowest.

When we compare the NBs in the HID, we see that the branch width changes with overall intensity. In the high level the NB is broader than in the medium level. The NB in the intermediate level is only broad in its upper part. Comparing the hard colour curves (Figs. 2c and f), we see that the character of the motion through the NB depends on intensity level. In the medium level the colours change slower than in the high level. These two new results are discussed in the next section.

3.1.7. The motion through the Z using S_z

The S_z parametrization makes it possible to investigate the kinematics of the motion along the Z track in more detail (see Dieters & van der Klis 1996). When examining S_z as a function of time it is evident that the source does not jump through the branches, but moves smoothly along the Z track. In the high level Cygnus X-2 seems to move faster up and down the normal branch than when the over-

all intensities are lower (compare Figs. 2c and f). In order to investigate this we calculated the velocity (V_z) and acceleration (A_z) distributions (Sect. 2.3; Dieters & van der Klis 1996). We find that the distributions are symmetric about zero : there is no difference in the motion up and down the Z track. The scatter of V_z and A_z increases from the HB, through the NB, to the FB indicating that the source moves through the Z most slowly on the HB, faster on the NB and fastest on the FB. On the NB the scatter of V_z and A_z increases when the overall intensity increases. In order to quantify this we determined the standard deviations of V_z (σ_{V_z}) and A_z (σ_{A_z}).

On the NB, σ_{V_z} and σ_{A_z} show a strong correlation with overall intensity (see Figs. 7a and b). They increase by a factor ~ 1.4 and ~ 1.5 , respectively, when the overall intensity increases by a factor of 1.34. No correlations between σ_{V_z} and σ_{A_z} on the FB and the overall intensity were found. For the HB the data do not allow a conclusion on this point.

In order to examine the width of the NB in the HID we applied the S_z parametrization on the Z track in the HID (Sect. 2.3). The D_z^{hid} time series are symmetric around zero. The lack of points on the HBs and FBs makes a definitive conclusion about the evolution of the width of the Z from the HB, via the NB to the FB, impossible. However, when two or more branches are present the Z width seems to increase from the HB to the NB, and further on the FB. As mentioned earlier (Sect. 3.1.6) we find that the NB width in the HID increases when the overall intensity increases. This effect is visible as a strong increase in the standard deviation of D_z^{hid} on the NB, with overall intensity (Fig. 7c). When the overall intensity increases by a factor ~ 1.34 , the standard deviation of D_z^{hid} on the NB increases by a factor ~ 1.75 . On the other branches the standard deviation of D_z^{hid} stays approximately the same at all overall intensities. When we examine the NB width in the CDs we do not find any increase in the standard deviation of D_z with overall intensity : the NB has approximately the same width at all intensity levels in the CDs.

3.2. The 1989 and the 1990 observations

3.2.1. The MPC1 mode data

In order to be able to compare these observations roughly with the other observations, and because of the very broad photon energy channels of the MPC3 mode (see Sect. 2.2), we made CDs and HIDs of the MPC 1 data only. Because during the November 1990 observation the MPC1 mode was used only very briefly, we combined the October 1989 (dots) and November 1990 (crosses) data in Fig. 3. In both the CD and the HID the HB and the NB are clearly visible. No FB is present. An upward curve can be seen at the beginning of the HB during the October 1989 observation. Such an upward curve of the HB was previously reported

by Kuulkers et al. (1996a) in the 1985 EXOSAT observation on day 301/302. The colour points of the November 1990 observation are displaced with respect to the October 1989 data.

3.2.2. The MPC3 mode data

In order to include the MPC3 data and to find out on which part of the Z track the source was in during the November 1990 observation, we had to use different colours, with broader energy bands. For comparison we did the same for the October 1989 data. The energy bands used are given in Table 2. Figure 4 shows a clear HB and NB for the October 1989 data (dots), as before, and the curve upwards of the HB, although less pronounced. The November 1990 data (crosses) show only a HB which is shifted in colour with respect to the October 1989 data. No upward curve is visible in the November 1990 data.

3.2.3. The PC mode data

The October 1989 PC data CD and the HID (Fig. 6) show a NB, the hard vertex and parts of the HB. In the HID, the points (indicated by the H) on the HB with the lowest intensity and low hard colour are not on the HB in the CD. They are placed on the hard vertex in the CD. The fast timing behaviour would suggest that those points are at the left end of the HB (see Sect. 4.4)

3.2.4. Comparison of the 1989 and 1990 observations to the other observations

The 1989 and 1990 observations were performed using different energy bands as compared to the other observations. Therefore, we can not directly compare their overall intensity levels. However, if we assume that the difference in the total count rate between 2.3–18.6 keV and 2.9–19.0 keV is minor we see that the overall intensity of the October 1989 observation is about the same as for the June 1987 observations. There is no NB available for the November 1990 observation so no direct comparison with the other observations of the mean NB intensity can be made. However, the shift of the HB during this observation with respect to the October 1989 HB indicates that the overall intensity of the November 1990 observation was higher than the overall intensity of the October 1989 observation. Therefore, we conclude that the October 1989 observation was taken at an overall intensity level in between the medium and high level, and the November 1990 observation during a high level episode.

4. Results : the fast timing behaviour

The results of the power spectra analysis are shown in Tables 4 and 5.

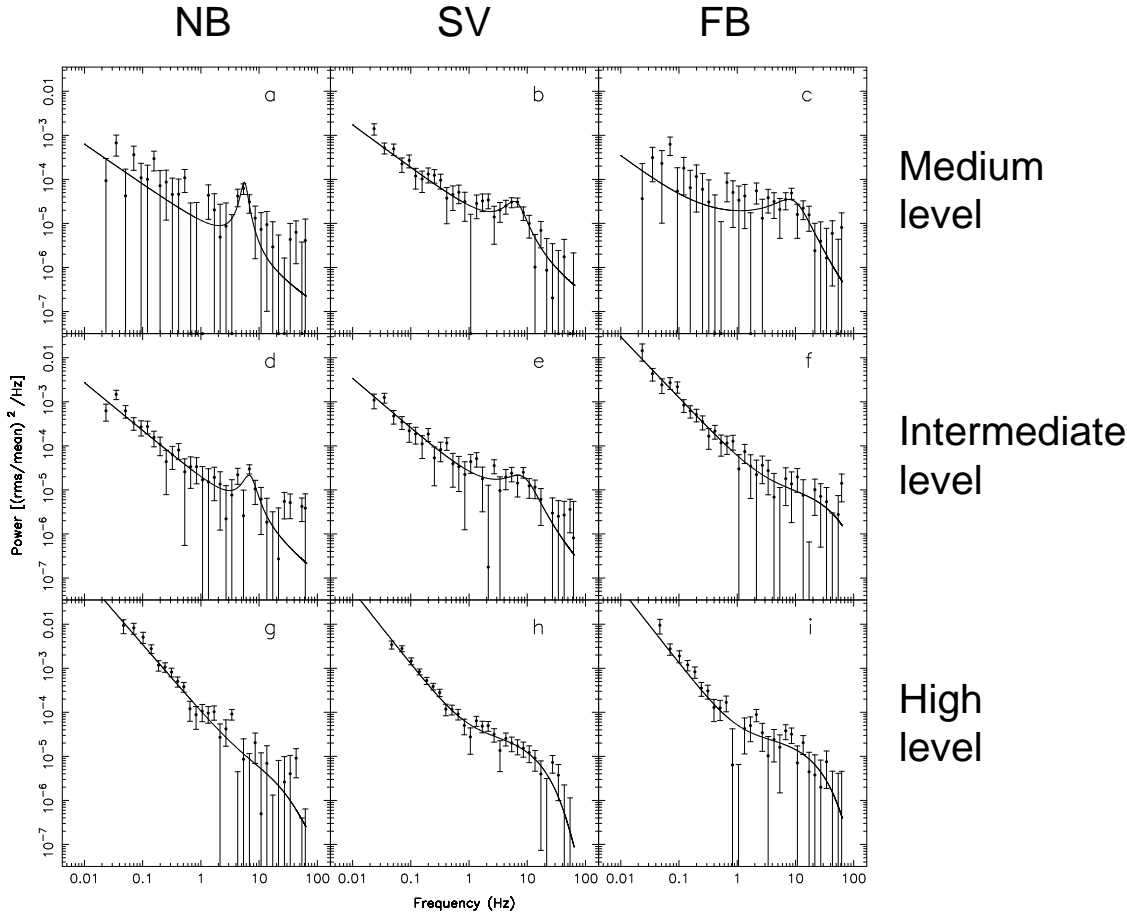


Fig. 8. Power spectra of different observations at about the same S_z , the power spectra in the column indicated with NB, SV and FB, are taken on the lower normal branch, the soft vertex, and the flaring branch, respectively: **a**, **b** and **c** are the May 1991 power spectra at $S_z=1.79\pm0.07$, 1.97 ± 0.10 and 2.05 ± 0.06 , respectively, **d**, **e** and **f** are the June 1987 power spectra at $S_z=1.83\pm0.02$, 1.97 ± 0.07 and 2.10 ± 0.03 , respectively, and **g**, **h** and **i** are the October 1988 power spectra at $S_z=1.856\pm0.008$, 2.00 ± 0.02 and 2.10 ± 0.01 , respectively

4.1. Very-low frequency noise (VLFN)

Since in the HB the VLFN is low (e.g. Hasinger & van der Klis 1989), we were in some cases unable to measure the VLFN, at the left end of the HB. In the June 1987 and June 1988 observations we fixed the power law index of the VLFN when Cygnus X-2 is on the HB.

We have high time resolution data of the same part of the Z track (especially near the soft vertex) but during different overall intensity levels. The comparison of these data reveals a very significant difference of the VLFN properties between the medium and high overall intensity levels in the lower part of the NB. During the medium overall intensity observations (June 1988 and May 1991) we detect a weak (0.5-1% rms amplitude) and flat (power law index of ~ 1) VLFN on the lower NB and near the soft vertex. The rms amplitude and power law index increase to $\sim 5.3\%$ and ~ 1.4 , respectively, on the upper FB in the

June 1988 observation. However, during the high overall intensity observations (October 1988 and June 1991) we detect a very strong (8.5% and 4.5% rms, respectively) and steep (index of 1.4-1.7) VLFN on the lower NB and near the soft vertex. The VLFN decreases in strength to about 6.7 % rms amplitude on the FB in the October 1988 observation. We note that this strong VLFN near the soft vertex can not be caused by changing collimator response. During the intermediate overall intensity observation (June 1987) we see VLFN with a strength of $\sim 1.5\%$ rms and power law index of ~ 1.1 near the soft vertex, which increases to $\sim 4.2\%$ and ~ 1.4 , respectively, on the FB. This gradual change in the strength and steepness of the VLFN as a function of overall intensity level is clearly visible in Figs. 8a-i. This figure shows the power spectra in the medium level, the intermediate level and the high level at approximately the same S_z values.

It is remarkable that when Cygnus X-2 is in the high level the VLFN near the soft vertex is strong and steep and that when the source is in the medium level the VLFN at the same S_z values is much weaker and less steep. During intermediate levels the VLFN is weak and flat on the NB but strong and steep on the FB. The correlation of the amplitude and steepness of the VLFN near the soft vertex with mean overall intensity level is not strict. At the highest overall intensities (1991 June) the amplitude is about the half of the one at the second highest overall intensity (1988 October), and the spectrum is less steep.

4.2. Low-frequency noise (LFN) and high-frequency noise (HFN)

Due to the scarcity of high time resolution data when Cygnus X-2 was on the HB or near the hard vertex and the difficulty in determining S_z , comparisons of the LFN between the observations are difficult. The June 1987 and 1988 observations show a LFN with an rms of $\sim 4.7\%$ on the HB which decreases to $\sim 3.0\%$ on the hard vertex and upper NB. The November 1990 observation shows that the rms of the LFN increases from the beginning of the HB to the hard vertex (from $\sim 5.8\%$ to $\sim 6.5\%$ rms). The same is seen in the October 1989 observation (LFN rms from 4.5% to 5.5%), but in this observation the rms decreases to 3.8% when the source moves into the upper NB. No clear correlation between the power law index ($0.0-0.3$) or the cut-off frequency ($4.0-13$ Hz) with S_z is seen.

When LFN or NBO were fitted it was difficult to fit the HFN simultaneously, possibly due to interference between them (see also Kuulkers et al. 1994a). When it was necessary to fit a HFN component it had an rms between $1-2\%$ and cut-off frequencies between 10 and 20 Hz. The October 1989 PC data show a strong HFN ($\sim 6\%$ rms) with a high cut-off frequency between 30 and 50 Hz.

4.3. Normal branch QPO (NBO)

Normal branch QPOs (NBOs) were detected in the medium and intermediate level observations. To our surprise, none were detected in the high level observations (see Fig. 8), although we had high timing data in the lower NB for them. The rms 2σ upper limits ($< 0.9\%$) are significantly lower than the rms ($1-2.5\%$) of the NBOs in the medium and intermediate levels. This also shows that during different overall intensity levels the rapid X-ray variability at the same position on the Z track differs significantly from each other.

When NBOs are seen no clear relation is detected between the amplitude of the NBO and S_z . However, the FWHM and the centroid frequency seems to increase from the middle of the NB to the FB. The FWHM increases from ~ 2.4 Hz to ~ 13 Hz and the centroid frequency from ~ 5 Hz to ~ 8 Hz. In the June 1987, the June 1988 and May 1991 observations it was impossible to make a dis-

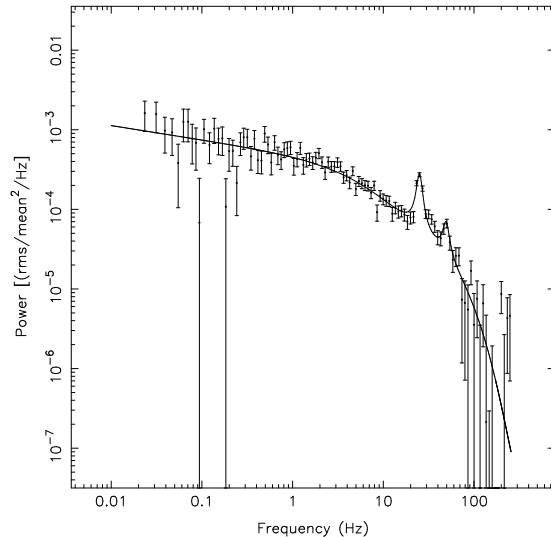


Fig. 9. The power spectrum of the beginning of the horizontal branch taken in the October 1989 observation. A harmonic of the HBO is visible at about 50 Hz

inction between a broad NBO or a HFN on the lower FB, although a NBO provided a better fit (e.g. for the June 1987 observation $\chi^2/\text{dof} = 27.5/29$ for the NBO versus $31.0/30$ for the HFN).

4.4. Horizontal branch QPO (HBO)

Horizontal branch QPOs are seen during all overall intensity levels, on the HB as well as in the upper NB. Taking all data into account, we find that the frequency of the HBO increases from ~ 31 Hz at the left end of the HB to ~ 55 Hz at the hard vertex. The PC data of the June 1987 and October 1989 observations indicate that when the source moves down the NB the HBO frequency decreases again to ~ 47 Hz. The rms amplitude decreases from the HB to the upper NB, from $\sim 4\%$ to $\sim 1\%$.

As already mentioned in Sect. 3.2.3, the PC data of October 1989 show several points at low intensities and high soft colour. Those points are placed in the CD near the hard vertex but in the HID near the left end of the HB. The power spectrum corresponding to these points is shown in Fig. 9. A HBO at 25 Hz is clearly visible (3.8% rms amplitude) and indicates that Cygnus X-2 was indeed at the left end of the HB (see Fig. 6, the points marked H). A second QPO is visible at ~ 49 Hz with a rms amplitude of 2.5% . Hasinger et al. (1985a) and Hasinger (1987) found already evidence for the harmonic of the HBO in the EXOSAT data of Cygnus X-2. However, the frequency ratio was smaller (1.85 ± 0.03) than expected for a second harmonic. Our frequency ratio (1.96 ± 0.05) indicates that this feature is indeed the second harmonic of the HBO.

Table 3. Bursts

No.	Date	Start (UT)	t_{burst} (s)	Mode	Time res. (s)	S_z	Orbital phase ^a	α	γ	τ (s)
I	1988-06-12	03:56:34	~ 8	MPC2	2	1.000	0.33	>105	1.92	3.66
II	1988-06-12	10:25:52	~ 4	MPC2	2	0.931	0.36	>94	3.52	2.00
III	1988-06-13	10:47:27	~ 8	MPC2	0.0625	1.229	0.47	>4.1	0.63	1.51
IV	1988-10-06	02:32:25	~ 2	MPC2	0.0625	1.222	0.11	>13.3	1.74	1.09
V	1989-10-22	08:04:47	~ 4	MPC1	4	1.4–1.5 ^b	0.84	>105	2.67	4.00

^a X-ray phase using the ephemeris given by Crampton & Cowley (1980), see Kuulkers et al. (1996a) note 4.

^b Only an estimate of S_z , due to the lack of a soft vertex.

5. Results: the bursts

We found five 2–8 s bursts similar to the burst-like events reported by Kuulkers et al. (1995). The times and the properties are given in Table 3. In Figs. 1c and e and Fig. 3a it is indicated where in the Z track the bursts occurred. The occurrence of the burst seems to be uncorrelated with the overall intensity level, the orbital phase, or the location in the Z track (although no burst were detected on the FB).

For the ratio, α , of the average persistent flux to the time-averaged flux emitted in the bursts (which reflects the ratio between the gravitational and nuclear burning energy per gram of accreted matter for thermonuclear bursts), we could only obtain lower limits (Table 3), since there are many interruptions by SAA and/or Earth occultations. They were calculated using the average count rate from the start of the last data gap to just before the burst. The other typical burst parameters γ , the ratio of the mean persistent pre-burst flux and net peak burst flux, and τ , the ratio of the total integrated net burst flux and the net burst peak flux (a representation of the burst duration) were also calculated (see Table 3). The count rates used in order to calculate the burst parameters were corrected for deadtime, background and aspect. Burst IV was observed during time when the satellite was slewing to the source. Therefore, during that time the collimator transmission was low ($\lesssim 50\%$) and the uncertainty on the count rate large. The count rate for burst IV was not corrected for the overestimation of the count rates in the low photon energy bands, due to the reflection of low energy photons (below 6 keV) against the collimator walls (see Sect. 2.1).

Due to the low time resolution of the data obtained during the occurrence of bursts I, II and V, we did not examine the burst profiles and spectral properties of these events. The burst profiles, for different energy bands, of bursts III and IV are shown in Figs. 10 and 11, respectively. These bursts do not show evidence for spectral cooling as would expected for bona fide type I bursts. Instead, it is clearly visible that burst III shows evidence for spectral hardening: the higher the energies, the broader the

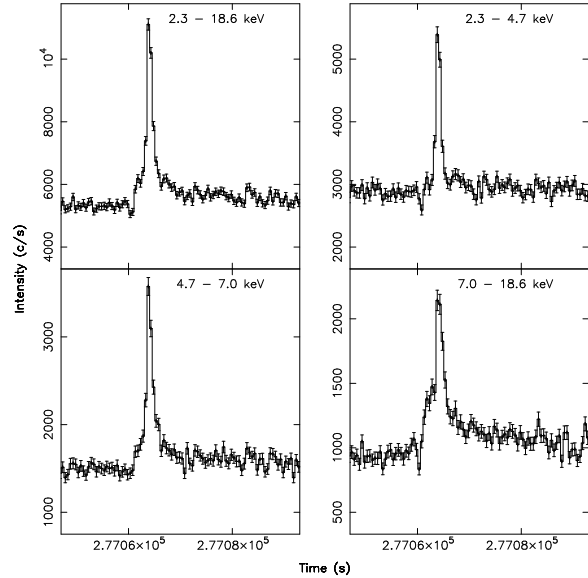


Fig. 10. The June 1988 burst (III) in the MPC2 high bitrate mode, time resolution is 0.5 seconds. Time is given from the beginning of the observation

event. Also, the post-burst count rate is higher than the pre-burst count rate. This effect is most prominent at the higher energies. Although these phenomena are not seen during event IV, no evidence for spectral cooling is seen either. In the nine bursts in the EXOSAT data of Cygnus X-2 hints for spectral hardening were already found (Kuulkers et al. 1995), although the poor statistics made a definite conclusion impossible. Taking all bursts into account we conclude that these events are probably not bona fide type I. We searched for QPOs and periodic oscillations during burst III and IV and found none. Statistics were insufficient to set meaning full upper limits.

6. Discussion

We have found several characteristics in the behaviour of Cygnus X-2 which seem to depend on overall intensity level. In the following we discuss some of those charac-

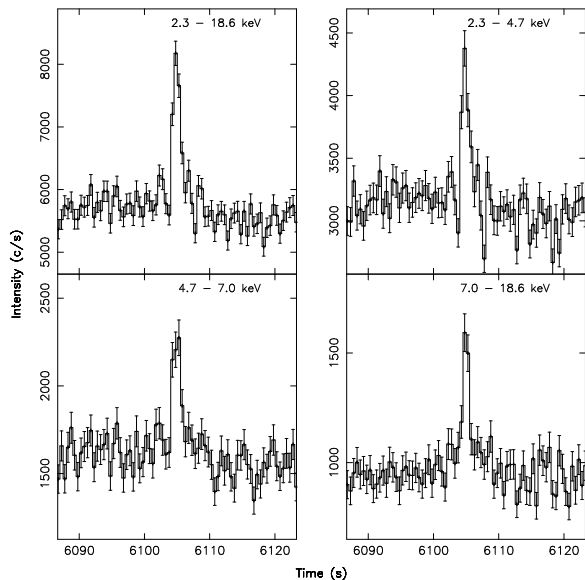


Fig. 11. The October 1988 burst (IV) in the MPC2 high bi-rate mode, time resolution is 0.5 seconds. Time is given from the beginning of the observation

teristics in more detail and suggest possible explanations for the different overall intensity levels and associated phenomena.

6.1. The rapid X-ray variability during different overall intensity levels

We find conclusive evidence that the rapid X-ray variability at the same point on the NB differs between different observations. We find a different kind of high timing behaviour near the soft vertex when Cygnus X-2 is in the medium level and the high level (see Fig. 8). In the medium level weak, flat VLFN is detected and a pronounced NBO occurs. In the high level the VLFN is stronger and steeper, and the NBO is not detectable. In the intermediate intensity level, the VLFN is strong and steep in the FB, but weak and flat in the NB, and the NBO is about the same strength as during the medium level. Our results are the first unambiguous detection of differences in the rapid X-ray variability at a specific position in the Z track (near the soft vertex) between different observations (see Dieters & van der Klis 1996 for a study of Sco X-1 with respect to this issue). So far, we find no evidence for any difference between the properties of the X-ray variability during different intensity levels on other parts of the Z track (such as the HB). However, our data do not allow a very detailed comparison of the timing behaviour on those parts of the Z track.

It is thought (van der Klis et al. 1985, 1987; Hasinger & van der Klis 1989; Lamb 1991) that variations in \dot{M} are responsible for the changes in the rapid X-ray variability

along the Z and the formation of the Z track, and that for this reason the rapid X-ray variability is closely related to the position of the source on the Z track. However, the shifting and shape changing of the Z track in Cygnus X-2 and other Z sources suggest that variations in \dot{M} can not explain all aspects of the formation of the Z track. We, therefore, suggest that both the shape of the Z track and the rapid X-ray variability are not totally determined by the mass accretion rate onto the compact object, but also partly by a so far unknown process, which may also cause the long-term intensity variations (see Sect. 6.4).

Two other Z sources, GX 5-1 and GX 340+0, display motion of their Z track in the CD (Kuulkers et al. 1994a; Kuulkers & van der Klis 1996), although not as pronounced as Cygnus X-2. Kuulkers et al. (1994a) and Kuulkers & van der Klis (1996) did not find any significant changes in the rapid X-ray variability in GX 5-1 and GX 340+0, respectively, when the Z track moved through the CD and HID. If the motion of the Z track in the CD and HID in Cygnus X-2, GX 5-1, GX 340+0 are caused by the same phenomenon, we then predict that the rapid X-ray variability in GX 5-1 and GX 340+0 changes when the Z tracks of those sources move through the diagram. The reason why so far no changes have been found is most likely due to the much lower amplitude of the motion of the Z through the CD and HID of GX 5-1 and GX 340+0, as compared to Cygnus X-2, which suggest that the amplitude of the difference of the rapid X-ray variability would also be much smaller. Moreover, in Cygnus X-2 so far only differences in the rapid X-ray variability were found near the soft vertex and not on e.g. the HB, while GX 5-1 and GX 340+0 were mainly observed in the HB and upper NB, and hardly near the soft vertex. Kuulkers et al. (1994a) and Kuulkers & van der Klis (1996) could not make a good comparison of the rapid X-ray variability near the soft vertex when the Z track of GX 5-1 and GX 340+0, respectively, moved in the CD and HID.

6.2. Velocity of motion along the Z track

Van der Klis (1991) suggested that the VLFN could be (partly) due to motion of the source along the Z track. In our analysis, we found that both the VLFN fractional amplitude and the velocity of motion along the Z track increase when the overall intensity level increases. However, the strongest VLFN was not observed during the most extreme high level, but during the less extreme, slightly lower one, whereas the highest velocity was indeed observed during the most extreme high level. Therefore, we conclude that the motion along the Z track is at most only partly responsible for the VLFN. As differences in NB slope in the HID can not explain this, part of the intensity variations causing the VLFN must take place perpendicular to the NB.

The increase in velocity along the Z track when the overall intensity increases indicates that the spectrum

changes more rapidly during high level episodes than during medium level episodes. If the Z track is traced out by changes in the mass accretion rate onto the neutron star, then an increase in the velocity of motion along the Z track indicates that \dot{M} changes more rapidly when the overall intensity level increases. However, it then seems unlikely that variations in \dot{M} can explain the shifts and changes in shape of the Z track between intensity levels (see also Sect. 6.1). It is possible that the increase in velocity of motion along the Z track is due to the same phenomenon causing the Z tracks to shift and the shapes to change.

6.3. The width of the NB in the HID

The width of the NB in the HID increases when the overall intensity increases, while the width of the NB in the CD remained approximately constant. This indicates that the difference in the width of the NB in the HID is due to intensity variations and not due to spectral variations. However, at the same time the velocity of motion along the Z track increases, which indicates an increase in spectral variations. So, in the HID, when the source moves perpendicular to the Z track (change in intensity), it also moves along the Z track (change in spectrum). Perhaps colours are well correlated with \dot{M} , but the intensity varies also due to another (unspecified) process that is more prominent in the high overall intensity level.

6.4. The overall intensity variations

Several models have been proposed (Priedhorsky & Holt 1987, and references therein) in order to explain long-term intensity variations in X-ray binaries, e.g. long-term variations in \dot{M} and precessing accretion disks. Precessing neutron stars have also been proposed to explain the variations (see Priedhorsky & Holt 1987; Schwarzenberg-Czerny 1992, and references therein).

6.4.1. Variations in the mass accretion rate

Long-term changes in the mass accretion rate have been proposed (see Priedhorsky & Holt 1987) to explain the long-term intensity variations in low-mass X-ray binaries other than Cygnus X-2 (e.g. 4U 1820-30, the Rapid Burster, Aql X-1, excluding Her X-1). However, Kuulkers et al. (1996a) and Wijnands et al. (1996b) argued that the long-term intensity variations in Cygnus X-2 can not be due to variations in the mass accretion rate. The main argument is that variations in the mass accretion rate are thought to produce motion of the source along the Z track (see e.g. Hasinger & van der Klis 1989), while the Z track is observed during several different intensity levels.

6.4.2. A precessing accretion disk

In order to explain long term intensity variations, not related to orbital variations, in high-mass X-ray binaries and

Her X-1, precessing accretion disks have been proposed (see Priedhorsky & Holt 1987 and references therein). The recent detection (Smale et al. 1996, Wijnands et al. 1996b) of a 78 day period in the RXTE, Vela 5B (see also Smale & Lochner 1992) and Ariel V all sky monitor data of Cygnus X-2 favours a precessing accretion disk in Cygnus X-2.

However, explaining the long-term X-ray variations of Cygnus X-2 with a precessing accretion disk is not without serious contradictions. If we assume that, during the medium overall intensity level, the emission region is blocked by (part of) the accretion disk and much radiation is absorbed, scattered and/or reflected, the power spectrum should be blurred and quasi-periodic oscillations (both the NBO and the HBO) should be harder to detect than when the emission region is not blocked by the accretion disk (the high level). However, we see exactly the opposite: no NBO is detected during high overall intensity levels. The upper limits are significantly lower than the actually detected values during the medium levels. If we assume that not during the medium level but during the high level the emission region is blocked by the accretion disk, then the difference between the power spectra are not totally unexpected. However, it is difficult to explain the increase of the count rate when the accretion disk is blocking our view of the emission region.

Another possibility is that the accretion disk blocks, during the medium overall intensity levels, a localised emission area (e.g. the neutron star surface), which is not blocked during the high levels. In this region no NBO occurs and therefore the fractional amplitude of the NBO during the high level is diluted by the additional flux. However, not only the strength of the NBO should be affected, but also the strength of the HBO, except when the HBO would originate from this localised area, in which case we would expect an inverse effect. This, however, is unlikely, because during all intensity levels HBOs are observed at approximately the same fractional amplitude.

Therefore, it is unlikely that the increase in count rates from the medium to the high level is caused by an localised emission region, which is sometimes hidden from our view by a precessing accretion disk, or by a precessing accretion disk, which sometimes blocks part of the total X-ray radiation.

Kuulkers et al. (1996a) proposed that the difference in overall count rates in the Cyg-like sources is caused by anisotropic emission, the radiation being scattered preferentially into the equatorial plane by a puffed-up inner disk structure. In this model, with increased scattering in the high level, the decrease in NBO amplitude follows naturally due to light travel time effects in the scattering process. Our observations therefore support their model.

6.4.3. A precessing neutron star

Another option is that the differences between the levels are due to changes in the properties of the emission region. A precessing neutron star could produce changes in the inner disk region. Due to the precession of the neutron star the orientation of the magnetic field with respect to the accretion disk changes. According to numerical calculations (Psaltis et al. 1995) the strength of the magnetic field is enough for the field to have a profound effect on the spectrum of the source and possibly also on the count rate. A change in the effective magnetic field, caused by a different orientation of the field, could maybe explain the different Z tracks during the different levels. Also, the rapid X-ray variability would be affected, although it is not clear if this could explain the differences that we found. The behaviour of the HBO should differ between the different intensity levels due to the different effective magnetic field, but no difference is found. It is also not clear why the NBO should differ between intensity levels.

6.5. The decrease of the HBO frequency down the NB

The decrease of the HBO frequency from the hard vertex down the NB in the June 1987 and October 1989 PC data allows us to apply the method described by Wijnands et al. (1996a), in order to derive an upper limit for the equatorial magnetic field strength. Assuming that the radius of the neutron star is $\sim 10^6$ cm we derive an upper limit of $\sim 8.5 \times 10^9$ G on the star's magnetic field at the magnetic equator. This value is similar to the value found for GX 17+2 (Wijnands et al. 1996a). This upper limit is consistent with numerical computations on the X-ray spectrum of Cygnus X-2 (Psaltis et al. 1995). As noted by Wijnands et al. (1996a), a further decrease of the frequency down the NB will reduce this upper limit. The fact that we see the HBO frequency decrease on the NB in Cygnus X-2 supports the interpretation that the QPO on the NB in GX 17+2, which also decreases in frequency (Wijnands et al. 1996a), is the HBO.

7. Conclusion

We observed Cygnus X-2 over a broad range of intensities. The source alternated between the known medium and high overall intensity levels and also sometimes in a state in between these two levels, both in intensity and other source characteristics. We found new correlations between several characteristics of the source and the overall intensity level :

- The velocity and acceleration along the normal branch increase when the overall intensity increases. During the high intensity level Cygnus X-2 moves faster and more irregularly up and down the normal branch than during lower levels.

- The width of the normal branch in the hardness-intensity diagram increases when the overall intensity increases.
- The very-low frequency noise near the soft vertex increases in amplitude and in steepness when the overall intensity increases.
- The normal branch quasi-periodic oscillation is not detectable ($\lesssim 0.9$ % rms) near the soft vertex when Cygnus X-2 is in the high level. During the other levels a NBO can be easily detected at a level of 1–2.5 % (rms).

The following correlations were already known and are confirmed by our analysis :

- The overall intensity changes with a factor of ~ 1.34 between the medium and the high overall intensity level.
- The shape of the Z-track in the colour-colour diagram and hardness-intensity diagram changes when the overall intensity changes. In the colour-colour diagram the horizontal and the flaring branch become more horizontal when the overall intensity increases. When the source enters the flaring branch during the medium overall intensity level the intensity first increases and later decreases. When the source enters the flaring branch during the high overall intensity level the intensity immediately starts to decrease.
- The whole Z-track shifts to softer colours when the overall intensity increases.

We also found several other previously unreported phenomena:

- Clear detection of overall intensity level episodes in between the medium and the high overall intensity level, indicating that the different overall intensity levels are part of a continuous range instead of a discrete set.
- The frequency of the horizontal branch quasi-periodic oscillation decreases down the NB, giving a model dependent upper limit on the magnetic field strength at the magnetic equator of $\sim 8.5 \times 10^9$ G.
- Detection of five bursts in the Ginga data, which do not show the characteristics of bona fide type I bursts.

Acknowledgements. This work was supported in part by the Netherlands Organization for Scientific Research (NWO) under grant PGS 78-277 and by the Netherlands Foundation for Research in Astronomy (ASTRON) under grant PGS 781-76-017. EK acknowledge receipts of an ESA fellowship.

A. Calculating the standard deviation of sample standard deviations

For the sample x_1, x_2, \dots, x_n let

$$\bar{x} = \text{mean} = \sum_{i=1}^n x_i / n \quad (\text{A1})$$

The sample standard deviation (s) is defined by

$$s = \left(\sum_{i=1}^n \frac{(x_i - \bar{x})^2}{n} \right)^{\frac{1}{2}} \quad (\text{A2})$$

The standard deviation of sample standard deviations is defined by (Burington & May 1970)

$$\sigma_s = \left[\frac{n-1}{n} - [b(n)]^2 \right]^{\frac{1}{2}} \sigma_x \quad (\text{A3})$$

with σ_x^2 the variance of the population given by the unbiased estimate $s^2 n / (n-1)$, $b(n) = (\frac{2}{n})^{\frac{1}{2}} \Gamma(\frac{n}{2}) / \Gamma(\frac{n-1}{2})$ and n the total number of points.

References

- Burington R.S., May D.C., 1970, Handbook of probability and statistics, with tables, second edition, Mc Graw-Hill New York-London, p.177
- Bowyer S., Byram E.T., Chubb T.A., Friedman H., 1965, Science 17, 894
- Crampton D., Crowler A.P., 1980, PASP 92, 147
- Dieters S., van der Klis M., 1996, A&A submitted
- Hasinger G., 1987, In: Helfand D.J., Huang Z. (eds.) The Origin and Evolution of Neutron stars, IAU 125, p.333
- Hasinger G., 1988, In: Tanaka Y. (ed.) Physics of Neutron Stars and Black Holes, p.97
- Hasinger G., van der Klis M., 1989, A&A 225, 79
- Hasinger G., Langmeier A., Sztajno M., Pietsch W., Gottwald M., 1985a, IAU Circ. 4153
- Hasinger G., Langmeier A., Pietsch W., Sztajno M., 1985b, Sp.Sc.Re. 40, 233
- Hasinger G., van der Klis M., Ebisawa K., Dotani T., Mitsuda K., 1990, A&A 235, 131
- Hertz P., Vaughan B., Wood K.S., et al., 1992, ApJ 396, 201
- Hoffman J. A., Marshall H. L., Lewin W. H. G., 1978, Nat 271, 630
- Kahn S.M., Grindlay J.E., 1984, ApJ 281, 826
- Kuulkers E., van der Klis M., 1995a, A&A 303, 801
- Kuulkers E., van der Klis M. 1995b, In: Böhringer H., Morfill G.E., Trümper J.E. (eds.) Seventeenth Texas Symposium on Relativistic Astrophysics and Cosmology, Ann. New York Ac. Sci. 759, p.344
- Kuulkers E., van der Klis M., 1996, A&A 314, 567
- Kuulkers E., van der Klis M., Oosterbroek T., et al., 1994a, A&A 289, 795
- Kuulkers E., van der Klis M., Oosterbroek T., van Paradijs J., Lewin W.H.G., 1994b, In: Holt S.S., Day C.S. (eds.) The Evolution of X-ray Binaries, American Institute of Physics, p.539
- Kuulkers E., van der Klis M., van Paradijs J., 1995, ApJ 450, 748
- Kuulkers E., van der Klis M., Vaughan B.A., 1996a, A&A 311, 197
- Kuulkers E., van der Klis M., Oosterbroek T., van Paradijs J., Lewin W.H.G., 1996b, MNRAS in press
- Lamb F.K., 1991, In: Ventura J., Pines D. (eds.) Neutron Stars: Theory and Observations, Kluwer, Dordrecht, NATO ASI Series C, 344, p.445
- Makino F., the ASTRO-C team 1987, Ap. Lett. Comm. 25, 223
- Mitsuda K., Dotani T., 1989, PASJ 41, 557
- Priedhorsky W.C., Holt S.S., 1987, Sp.Sc.Re. 45, 291
- Psaltis D., Lamb F.K., Miller G., 1995, ApJ 454, L137
- Schwarzenberg-Czerny A., 1992, A&A 260, 268
- Smale A. P., Lochner J. C., 1992, ApJ 395, 582
- Smale A. P., Kuulkers E., Wijnands R. A. D., 1996, IAU Circ. 6452
- Sztajno M., Langmeier A., Trümper J., van Paradijs J., Lewin W.H.G., 1986, MNRAS 222, 499
- Tawara Y., Hirano T., Kii T., Matsuoka M., Murakami T., 1984, PASJ 36, 861
- Turner M.J.L., Thomas H.D., Patchett B.E., et al., 1989, PASJ 41, 345
- van der Klis M., 1991, In: Ventura J., Pines D. (eds.) Neutron Stars : Theory and Observations, Kluwer, Dordrecht, NATO ASI Series C 344, p.27
- van der Klis M., Jansen F., van Paradijs J., van den Heuvel E. P. J., Lewin W. H. G., 1985, Nat 316, 225
- van der Klis M., Jansen F., van Paradijs J., et al., 1987, ApJ 313, L19
- Vrtilek S.D., Kahn S.M., Grindlay L.E., Seward F.D., Helfand D.J., 1986, ApJ 307, 698
- Vrtilek S.D., Swank J.H., Kelly R.L., Kahn S.M., 1988, ApJ 329, 276
- Wijnands R. A. D., van der Klis M., Kuulkers E., et al., 1996a, ApJ 469, L5
- Wijnands R. A. D., Kuulkers E., Smale A. P., 1996b, ApJ 473, L45

Table 4: Results of power spectral fits of the MPC3 data^a

Observation	S_{\pm}^c	VLFN		LFN			NBO			HBO			HFN		χ^2	DOF
		rms %	α	rms %	α	ν Hz	rms %	$\Delta\nu$ Hz	ν Hz	rms %	$\Delta\nu$ Hz	ν Hz	rms % Hz	ν		
7 June	1.19±0.01	2.59±0.16	1.50 ^b	3.04±0.08	0.30±0.06	11.0 ^{+1.9} _{-1.5}				1.74±0.10	12.7 ^b	49.1±1.0			116.0	83
	1.60±0.01	1.77±0.10	1.02±0.05				1.56±0.12	2.38±0.46	5.36±0.17	1.02 ^{+0.24} _{-0.16}	4.8 ^{+4.9} _{-15.1}	52.4 ^{+2.7} _{-0.9}			83.5	82
	1.83±0.02	1.31±0.13	1.09±0.12				1.09±0.29	4.0 ^{+3.5} _{-2.8}	6.74 ^{+0.88} _{-0.68}						53.5	44
	1.97±0.07	1.45±0.19	1.13±0.15				1.81 ^{+0.47} _{-0.32}	10.7 ^{+6.4} _{-4.1}	7.1 ^{+1.5} _{-2.6}						27.5	29
	2.10±0.03	4.19 ^{+0.83} _{-0.57}	1.39±0.12										1.76 ^{+0.68} _{-0.40}	32.1 ^{+∞} _{-22.3}	21.1	30
8 June	0.95±0.01	1.06±0.24	1.00 ^b	4.73±0.12	0.21±0.06	13.1 ^{+1.9} _{-1.6}				1.24±0.32	7.7 ^{+6.2} _{-3.6}	54.0±2.3			57.6	70
	1.16±0.03	1.11±0.23	1.00 ^b	3.02±0.15	0.12±0.13	5.4 ^{+1.4} _{-1.1}				1.87±0.30	12.7 ^{+7.3} _{-5.3}	54.5±2.0			70.2	70
	1.38±0.03	1.69±0.10	0.79±0.07				1.65 ^{+0.56} _{-0.34}	3.1 ^{+2.7} _{-1.5}	4.79 ^{+0.51} _{-0.87}						23.6	44
	2.37±0.02	2.17 ^{+1.40} _{-0.43}	1.50±0.35										2.20±0.33	14.0 ^{+9.1} _{-6.0}	48.8	45
	2.72±0.03	2.38±0.24	1.05±0.13										1.58 ^{+0.48} _{-0.64}	15.00 ^b	44.0	31
8 October	1.856±0.008	8.5 ^{+1.8} _{-1.3}	1.53±0.10				<0.87	3.00 ^b	5.5 ^b				0.87±0.77	15.00 ^b	52.2	54
	2.00±0.02	6.35 ^{+1.10} _{-0.78}	1.67±0.09				<0.76	6.00 ^b	6.0 ^b				1.78±0.14	10.3 ^{+3.0} _{-2.3}	62.7	77
	2.10±0.01	6.7 ^{+1.6} _{-1.1}	1.69±0.13				<1.60	12.00 ^b	7.0 ^b				2.00±0.30	14.9 ^{+8.3} _{-4.8}	52.2	53
1 May	1.79±0.07	0.70±0.15	0.91 ^{+0.44} _{-0.26}				1.45±0.23	1.57 ^{+0.81} _{-0.52}	5.57±0.22						47.0	58
	1.97±0.10	1.11±0.07	0.98±0.10				1.56±0.25	5.5 ^{+2.4} _{-1.7}	5.98 ^{+0.58} _{-0.68}						63.2	85
	2.05±0.06	0.48±0.21	1.00 ^b				2.60 ^{+0.52} _{-0.35}	12.5 ^{+7.7} _{-4.4}	7.7 ^{+1.5} _{-2.0}						41.8	59
1 June	1.74±0.03	3.95 ^{+0.46} _{-0.37}	1.39±0.08				<0.84	3.00 ^b	5.5 ^b				1.22±0.38	14.9 ^{+37.3} _{-8.8}	49.0	59
	1.95±0.01	4.46±0.35	1.57±0.05				<0.84	6.00 ^b	6.0 ^b				1.75±0.20	26.6 ^{+15.3} _{-7.8}	67.7	59
0 November	3.624 < Int < 3.670			5.79±0.17	0.01±0.06	6.69 ^{+1.02} _{-0.84}				3.84±0.35	10.5 ^{+2.8} _{-2.0}	31.01±0.83			63.3	57
	3.675 < Int < 3.701			5.76±0.23	0.08±0.07	8.0 ^{+1.7} _{-1.3}				4.05 ^{+0.71} _{-0.50}	13.5 ^{+8.4} _{-4.5}	33.7 ^{+1.5} _{-1.0}			58.7	57
	3.702 < Int < 3.717			6.26±0.18	0.26±0.05	10.2 ^{+1.7} _{-1.4}				3.72±0.50	20.6 ^{+7.7} _{-5.3}	41.3±2.2			50.4	57
	3.717 < Int < 3.738			6.49±0.08	0.31±0.02	11.23±0.79				2.52±0.24	11.4 ^{+3.3} _{-2.5}	41.03±0.85			66.3	81

All errors are determined from an error scan through the χ^2 space using $\Delta\chi^2 = 1$. Whenever no value of a component is given, this component was not significantly detected in the average power spectrum..

Parameter fixed.

The error is defined as the standard deviation in the mean of the S_{\pm} points in the chosen segment. If no S_{\pm} value could be determined the chosen intensity (Int) range is indicated.

Table 5: Results of power spectral fits of the PC data^a

Observation	S_z	VLFN		LFN		NBO			HBO			HFN		χ^2	DOF	
		rms %	α	rms %	α	ν Hz	rms %	$\Delta\nu$ Hz	ν Hz	rms %	$\Delta\nu$ Hz	ν Hz	rms % Hz			ν
7 June	0.457 <SC< 0.467	2.32±0.13	0.84±0.05				2.34±0.22	2.89 ^{+0.75} _{-0.58}	5.00±0.19	1.58 ^{+0.33} _{-0.21}	5.6 ^{+5.1} _{-4.6}	52.2 ^{+0.8} _{-1.3}		97.0	100	
	-0.918 <HC< -0.893															
	0.446 <SC< 0.455	2.17±0.15	0.90±0.07				2.21±0.28	3.4 ^{+1.1} _{-0.9}	5.02±0.25	1.66±0.35	10.3±6.8	54.8 ^{+2.0} _{-2.4}		93.5	100	
	-0.947 <HC< -0.923															
	0.435 <SC< 0.444	1.96±0.15	0.84±0.07				1.95±0.15	1.83±0.34	5.30±0.13	1.50 ^{+0.44} _{-0.30}	9.5 ^{+9.2} _{-3.8}	54.3±2.0		129.0	100	
	-0.974 <HC< -0.951															
	0.421 <SC< 0.434	2.42±0.17	1.12±0.07				2.06±0.16	3.60 ^{+0.71} _{-0.60}	5.61±0.22	1.88±0.27	18.8 ^{+8.5} _{-6.3}	51.0 ^{+2.6} _{-3.0}		60.8	84	
-1.003 <HC< -0.975																
0.387 <SC< 0.415	0.89±0.16	0.60±0.14				<1.18	3.50 ^b	5.50 ^b					36.3	38		
-1.051 <HC< -1.015																
8 June	0.97±0.02	1.25±0.26	1.50 ^b	4.07±0.09	0.34±0.04	11.4 ^{+1.7} _{-1.5}				2.66±0.22	20.3 ^{+6.0} _{-4.2}	54.5 ^{+1.2} _{-1.4}		116.0	101	
	1.31±0.04	1.61±0.06	0.78±0.03				2.46±0.12	2.46±0.32	5.53±0.09	1.45±0.22	7.6±3.1	54.1±1.4		99.5	100	
	1.54±0.05	0.95±0.10	0.75±0.10				2.76±0.13	1.64±0.24	5.78±0.07					76.9	70	
	1.940±0.004	1.25±0.10	1.01±0.12				2.30±0.28	10.2 ^{+3.3} _{-2.5}	8.20±0.92					78.6	70	
	2.16±0.24	2.03 ^{+1.45} _{-0.44}	1.38±0.39										2.58±0.48	19.3 ^{+23.4} _{-10.2}	8.24	13
	2.72±0.08	5.31 ^{+0.95} _{-0.68}	1.44±0.10										23.0 ^{+∞} _{-10.8}	14.3	21	
8 October	HV ^d	3.19 ^{+1.10} _{-0.54}	1.82±0.25	4.36±0.14	0.28±0.05	9.1±1.2				2.41±0.18	11.4 ^{+1.8} _{-1.7}	51.70±0.42	2.61±0.34	50.00 ^b	84.0	99
	SV	2.64±0.17	1.35±0.06				<0.90	6.00 ^b	6.00 ^b				2.24±0.09	13.4 ^{+1.8} _{-1.5}	102.0	88
	E	2.79 ^{+1.05} _{-0.53}	1.43±0.24										1.53±0.55	15.00 ^b	17.7	18
9 October	3.595 <Int< 3.670			4.50 ^{+0.41} _{-0.30}	0.20 ^b	6.14 ^{+1.12} _{-0.82}	2.48 ^{+0.82} _{-0.36}	8.9 ^{+7.3} _{-2.8}	49.19 ^{+0.81} _{-1.09}	3.83±0.21	4.12±0.57	25.05±0.18	5.78 ^{+0.42} _{-0.66}	33.6±5.1	161.0	114
	-0.550 <HC< -0.525															
	3.61 <Int< 3.68			4.70 ^{+0.75} _{-0.61}	0.20 ^b	8.2 ^{+2.6} _{-2.0}				3.24 ^{+0.47} _{-0.34}	3.4 ^{+3.7} _{-2.7}	32.98 ^{+0.35} _{-0.56}	6.39 ^{+0.65} _{-0.80}	46.7 ^{+15.0} _{-9.6}	50.3	68
	-0.520 <HC< -0.503															
	3.785 <Int< 3.850			5.98±0.13	0.35±0.03	13.6 ^{+2.0} _{-1.7}				3.53 ^{+0.41} _{-0.33}	19.3 ^{+7.6} _{-4.9}	53.3±1.2		103.0	86	
	-0.534 <HC< -0.520															
	3.828 <Int< 3.897	2.22±0.16	1.00 ^b	3.90±0.13	0.14±0.08	10.4 ^{+1.6} _{-1.3}				2.79±0.12	11.2 ^{+1.5} _{-1.4}	52.13±0.43		122.0	101	
	-0.547 <HC< -0.529															
3.800 <Int< 3.880	2.30 ^{+1.07} _{-0.10}	0.88±0.05				2.03 ^{+0.33} _{-0.24}	4.7 ^{+1.6} _{-1.2}	5.10±0.39	1.91±0.30	16.4 ^{+6.7} _{-6.1}	46.8±2.4		42.3	50		
-0.570 <HC< -0.580																

All errors are determined from an error scan through the χ^2 space using $\Delta\chi^2 = 1$. Whenever no value of a component is given, this component was not significantly detected in the average power spectrum.

Parameter fixed.

The error is defined as the standard deviation in the mean of the S_z points in the chosen segment. If no S_z value could be determined the chosen intensity (Int), soft colour (SC), or hard colour (HC) range is indicated.

The power spectra of the October 1988 observation indicated with HV, SV, and E were calculated for the area given by HV, SV, and E, respectively, in Fig. 5e.